Hindawi
Advances in Materials Science and Engineering
Volume 2018, Article ID 9843416, 13 pages
https://doi.org/10.1155/2018/9843416

Research Article

Energy Evolution Behavior and Mesodamage Mechanism of Crumb Rubber Concrete

Shengtong Di,[1,2,3] **Chao Jia**,[2] **Weiguo Qiao**,[3,4] **Kang Li**,[1,2] **and Kai Tong**[1,2]

[1]*School of Civil Engineering, Shandong University, Jinan, Shandong 250061, China*
[2]*Institute of Marine Science and Technology, Shandong University, Qingdao, Shandong 266237, China*
[3]*Key Laboratory of Disaster Prevention and Reduction of Civil Engineering in Shandong Province, Qingdao, Shandong 266590, China*
[4]*School of Civil Engineering and Architecture, Shandong University of Science and Technology, Qingdao, Shandong 266590, China*

Correspondence should be addressed to Chao Jia; jiachao@sdu.edu.cn

Received 21 August 2018; Revised 2 December 2018; Accepted 10 December 2018; Published 26 December 2018

Academic Editor: Alicia E. Ares

The energy evolution behaviour and mesodamage mechanism of CRC (crumb rubber concrete) were investigated by laboratory experiments and numerical simulations. The mesoscopic physical and mechanical parameters of CRC (crumb rubber concrete) materials were analyzed and determined by the discrete element method and trial-and-error method, and the mechanism and evolution of microcracks propagation during CRC failure were studied based on the parallel-bond model. The relationship among dissipation energy, damage threshold, and rubber content during CRC damage was studied by adopting the method of microscopic energy tracking. The energy release ratio was proposed to analyze the degree of "brittleness" of CRC after reaching its peak strength. The essential mechanism of different failure characteristics of CRC and NC (normal concrete) was analyzed and discussed by referring to their correlation between the microenergy evolution rule and the constitutive curve. The results show that (1) the calibrated mesoscopic physical and mechanical parameters can better reflect the mechanical characteristics of CRC materials, (2) there is a strong correlation between the mesoscopic damage threshold of CRC with different rubber contents and the proportion of dissipation energy at the peak strength, and the damage threshold of the CRC with 25% rubber mass is the largest, (3) the relationship between elastic strain energy release ratio of CRC and rubber particle contents can be fitted by the negative exponential function, and (4) the essential reasons for the different destruction characteristics of CRC and NC is that the addition of rubber particles makes more external input energy to be converted into dissipative energy required for microcracks propagation and sliding friction between particles and released step by step.

1. Introduction

CRC (crumb rubber concrete), referred as elastic composite material concrete, has the excellent performance on light weight, elastic damping, ductility and toughness, and environmental protection. CRC has been broadly applied in the fields of road, highway, bridge deck, and underground engineering, while it often suffers damage and failure on a larger scale due to the generation and propagation of microcracks, which are often neglected. Therefore, understanding and mastering the mesodamage mechanism and failure rules of CRC materials is very important to ensure the quality and safety of the materials applied in engineering.

Current research often focuses on improving the overall strength, deformation, or impact resistance of CRC materials by designing better ratio schemes through laboratory tests, but ignores the occurrence and expansion process of material failure that often occurs in engineering. Eldin and Senouci [1], Khatib and Bayomy [2], and Yu and Zhu [3] conducted laboratory experiments to study the law of the physical and mechanical properties of composite material mixed with different sizes and different amounts of rubber particles. Segre and Joekes [4] and Wang et al. [5] studied the bonding effect of the rubber modified by chemical solution and obtained the properties of mortar-rubber interface and the physical and mechanical properties law of the aggregate

concrete. Topcu [6–8] carried out a series of researches on waste tire concrete, in which the physical and mechanical properties of the concrete at different ages were studied in detail by preparing samples with different size and dosage of rubber particles content. Hernandez-Olivares et al. [9] prepared aggregate concrete by adding the crushed tire rubber and polypropylene fiber of a certain volume fraction into the concrete and studied the cementation and compatibility of cement-rubber through SEM (scanning electron microscope), and the tensile and bending resistance tests and dynamic compression tests were performed at different curing times of samples. Youssf et al. [10] took the effect of rubber particles' preprocessing time, silicon powder content, and cement content on the amount of compression, compression strength, and tensile strength of CRC into account, and the best mix ratio that can improve the mechanical properties of CRC was obtained.

Zhu et al. [11–13] conducted extensive research on the mechanical properties of crumb rubber concrete and established a regression relationship between compressive strength, elastic modulus, and influencing factors, and the failure mechanism of crumb rubber concrete was discussed. Yang [14] made a theoretical and analytical exploration of CRC from the perspective of microstructure and application. Liu et al. [15–17] established an aggregate model of a random distribution by discretizing the CRC at a mesoscopic level and conducted a simulation study on the deformation of CRC based on the finite element method. Liu [18] studied the frost-resistance durability and microscopic frost-resistance mechanism of rubber concrete mixtures in different erosion media. Yuan and Zheng [19], Xu et al. [20], and Guo et al. [21] carried out the dynamic performance test of rubber concrete, respectively, and different impact resistance between ordinary concrete and CRC was analyzed.

However, the internal mesomechanical response processes and laws in materials cannot be revealed through conventional laboratory experiments. In addition, the limitations of laboratory conditions and the discrete physical-mechanical properties of the samples make it impossible to systematically understand and master the energy evolution rules and mesodamage mechanism of materials.

In the present study, the damage mechanism and energy evolution of CRC materials in the process of deformation and failure were studied from a microscopic perspective by referring to the particle discrete element method introduced by Cundall and Strack [22] in 1979. First, the deformation and failure characteristics of CRC with different rubber content were briefly described and analyzed, and the correlation between CRC strength, deformation parameters, and rubber content of CRC with different rubber content was obtained by data fitting method. Then, the micromechanical parameters of CRC composites were determined by inverse analysis based on the laboratory research results, and the rationality and validity of the micromechanical parameters were verified by the experimental results of other groups of samples. Next, the mechanism of generation and propagation of microcracks during CRC failure was analyzed, and the correlation between mesoscopic damage variable and dissipated energy at different stages was studied, and the evolution of CRC damage threshold with rubber content was discussed. And then, the energy release ratio is defined after the composite materials reach the peak strength, which is used to analyze and evaluate the flexibility and ductility of the composite concrete materials, and the energy release ratio of CRC with different rubber content was calculated and analyzed by data fitting. Finally, taking the CRC group with the maximum damage threshold as the representative, the essential mechanism of different failure characteristics of CRC and NC was discussed from the perspective of mesoscopic energy. This process can not only effectively solve the limitations caused by the laboratory test and the dispersion of experimental results, but also can provide useful reference and supplement for the study on mechanics, progressive deformation, and failure characteristics of composite materials.

2. Laboratory Experiment

2.1. Experimental Scheme. This test is mainly to study the effect of different blending content of rubber particles on the mechanical properties of CRC. The following materials were used in this work: P.O 42.5 cement and polyacrylate emulsion as binders; continuous grading ordinary sand with maximum size of 3 mm; rubber particles with a size of 3–5 mm; naphthalene superplasticizer as an admixture; and saturated sodium hydroxide solution (NaOH). The rubber particles were surface-pretreated with saturated NaOH solution at room temperature for 30 minutes while stirring. It not only removed dust particles on the rubber surface, but effectively decomposed carboxyl and acid-based components on the rubber surface [7]. The adhesion of rubber-mortar and the overall strength of the material were also enhanced. Rubber particles before and after surface-pretreated with NaOH saturated solution are shown in Figure 1.

According to the orthogonal test results of our previous work [23], the amount or proportion of materials used in samples are as follows: the cement dosage was 380 kg/m^3, the water/cement ratio was 0.35, the cement/aggregate ratio was 0.2, the water reducer dosage was 1.5% of the cement dosage, and the binder dosage was 15% of the rubber particle dosage. There were eight groups with different rubber content in the experiment, they were 0%, 5%, 10%, 15%, 20%, 25%, 30%, and 40% of the sample mass, and the group of 0% rubber content, that is, normal concrete, was used as the control group. Based on the mixing principle of materials, the mixing ratio of each group was determined as shown in Table 1. Then, the same preparation process was used to complete the samples preparation in the same laboratory environment, and the strength tests were conducted after curing in the standard curing room for 28 days.

The test specimen was the standard cylindrical shape with a specification of $\Phi 50\,\text{mm} \times 100\,\text{mm}$. Three specimens were prepared for each group and the average value was taken as the representative value of the corresponding mix proportion scheme.

The electrohydraulic servo compression testing machine was used to test the strength and deformation characteristics of the CRC. Figure 2 shows the loading process of CRC specimens, the loading rate is set to 0.1 mm/min.

(a) (b)

Figure 1: Rubber particles before and after surface-pretreated with NaOH saturated solution.

Table 1: Mix proportion of rubber concrete in experiment (unit: kg/m^3).

Number	Rubber	Cement	Sand	Water	Water reducer	Agglomerant
O	0	380	1900	133	5.7	0
A	120.9	380	1760.9	133	5.7	18.1
B	241.9	380	1621.9	133	5.7	36.3
C	362.8	380	1482.8	133	5.7	54.4
D	483.7	380	1343.7	133	5.7	72.6
E	604.7	380	1204.6	133	5.7	90.7
F	725.6	380	1065.6	133	5.7	108.8
H	967.5	380	787.4	133	5.7	145.1

Figure 2: Specimen under uniaxial compression test.

2.2. Experimental Results and Analysis. The typical failure form of uniaxial compression of each group is shown in Figure 3, and it can be seen that normal concrete shows shear failure of single sloping plane and no other obvious small cracks appear on the surface. Group A and B also show shear failure of single sloping plane with large perforative crack. With the increase of rubber particles content, the failure form of the samples from C to H was gradually changed from a form of single sloping and complete plane to a form of short and dispersed cracks. And the serial macrocrack began to disappear, and many fine discontinuous microcracks began to appear on the surface. The axial deformation of samples gradually increased, and the integrity of the sample was better after reaching its ultimate bearing capacity.

The correlation between the mechanical deformation parameters and the rubber particles content in every sample group is shown in Figure 4. It shows that the compressive strength of CRC is 69.9% lower than that of NC, and CRC has a slow decrease in compressive strength with the increase of rubber particles content. The fitting function $y_1 = (-9375 * x + 1.873e5)/(x^2 + 2.572e4 * x + 3.994e4)$ can be used to describe the relationship between the compressive strength and the rubber particles content, with a variance of 0.9917. With the increase of rubber particles content, the elastic modulus shows a similar attenuation trend as the compressive strength, and the elastic modulus of CRC has a decrease of 56.5% compared to that of NC. Compared with the trend of change in compressive strength, the decrease in elastic modulus is smaller and the downward trend is slower in the later period. The function $y_2 = (-3.691e8 * x + 5.985e8)/(x^2 + 3.692e5 * x + 6.994e5)$ can be used to fit and analyze the relationship between the elastic modulus and the rubber particles content, with a variance of 0.9848.

3. Numerical Simulation Experiment

3.1. Particle Discrete Element Method. Particle discrete element method is a particular implementation of a broader class of methods known as discrete element methods, which are defined as methods that allow finite displacements and rotations of discrete bodies, including complete detachment, and recognize new contacts automatically as the calculation progresses. The CRC material is simulated by a dense packing of non-uniform-sized spherical particles that are bonded together at their contact points, and its mechanical behavior is described by the movement of each particle and the force and moment acting at each contact based on Newton's second law and force-displacement law. The PBM (parallel-bond model) is implemented in the PFC3D using the DEM and can be used to simulate and analyze the conventional mechanics, deformation, and failure characteristics of rock and concrete [24]. The contact model and failure criterion are shown in Figure 5.

(a) (b) (c) (d) (e) (f) (g) (h)

Figure 3: The shape of the destruction (from left to right: O, A, B, C, D, E, F, H).

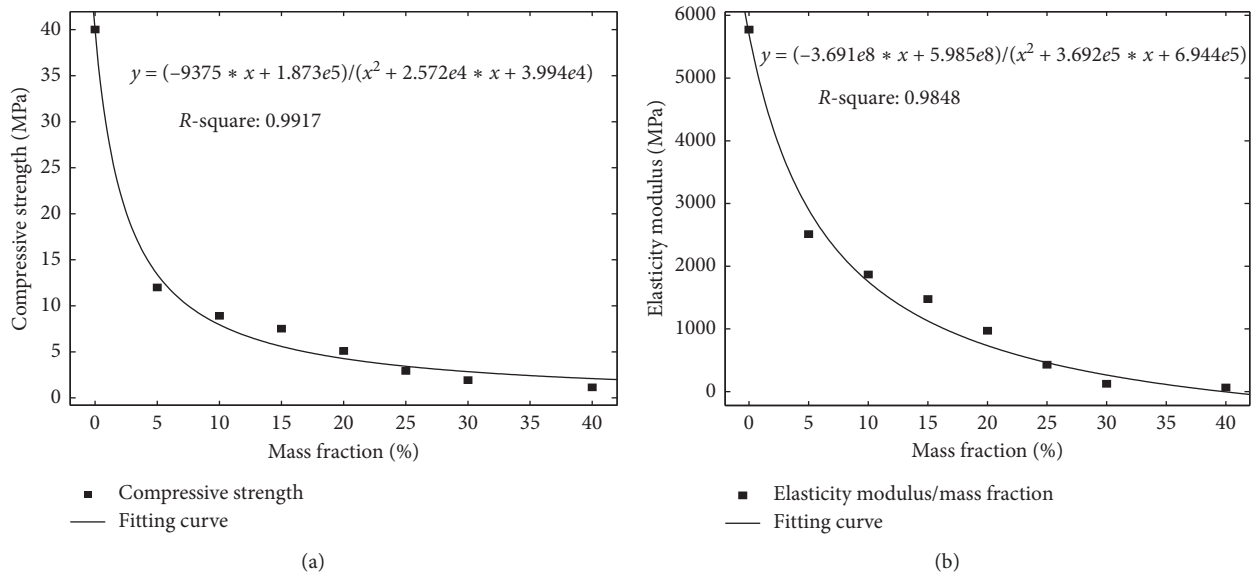

(a) (b)

Figure 4: The mechanical parameters and its curve fitting.

As shown in Figure 5, the PBM is composed of cemented substance and adjacent rigid particles, and its mechanical model consists of several mechanical components that have axial or tangential forces along the line joining the particle centers. In the axial direction, the normal linear contact force of particles is produced by linear springs with constant normal stiffness k_n, the normal dashpot force is produced by dashpots with normal viscous rheological β_n, the tensile strength $\overline{\sigma}_c$ of cement is produced by bonding block, and the normal linear contact force of cement is produced by the other linear springs with constant normal stiffness $\overline{k}_n$. In the tangential direction, the tangential linear contact force of particles is produced by linear springs with the tangential stiffness k_s, the tangential dashpot force is produced by dashpots with tangential viscous rheological β_s, the shearing strength $\overline{c}$ and $\overline{\Phi}$ of cement is produced by shear blocks, the tangential linear contact force of cement is produced by the other linear springs with constant tangential stiffness $\overline{k}_s$, and the friction between adjacent particles is produced by sliders with friction coefficient μ.

Under the action of load on both ends of the particles, the normal stress $\overline{\sigma}$ and tangential stress $\overline{\tau}$ of the bond in the parallel-bond model can be expressed, respectively, as

$$\overline{\sigma} = \frac{\overline{F}_n}{\overline{A}} + \overline{\beta}\frac{\left\|\overline{M}_b\right\|\overline{R}}{\overline{I}},$$
$$\overline{\tau} = \frac{\left\|\overline{F}_s\right\|}{\overline{A}} + \overline{\beta}\frac{\left|\overline{M}_t\right|\overline{R}}{\overline{J}}, \quad (1)$$

where the moment-contribution factor $\overline{\beta} \in [0, 1]$, $\overline{R}$ is the radius of bond, $\overline{A}$ is the cross-sectional area of bond, $\overline{I}$ is the inertia moment of bonding cross section, and $\overline{J}$ is the polar inertia moment of the cross section of bond. The force acting on the bond can be resolved into the normal force $\overline{F}_n$ and the tangent force $\overline{F}_s$, and the moment of bond can be resolved into the torsional moment $\overline{M}_t$ and the bending moment $\overline{M}_b$.

3.2. Numerical Simulation Scheme. In order to better simulate the mechanics and contact behavior between particles in the CRC, the three-dimensional numerical models with different rubber particles content were established according to the size of the laboratory samples, and its specification was Φ50 mm × 100 mm. The yellow particles in models represent the sands with the minimum radius of 0.8 mm, and the black particles represent the rubber particles with the minimum

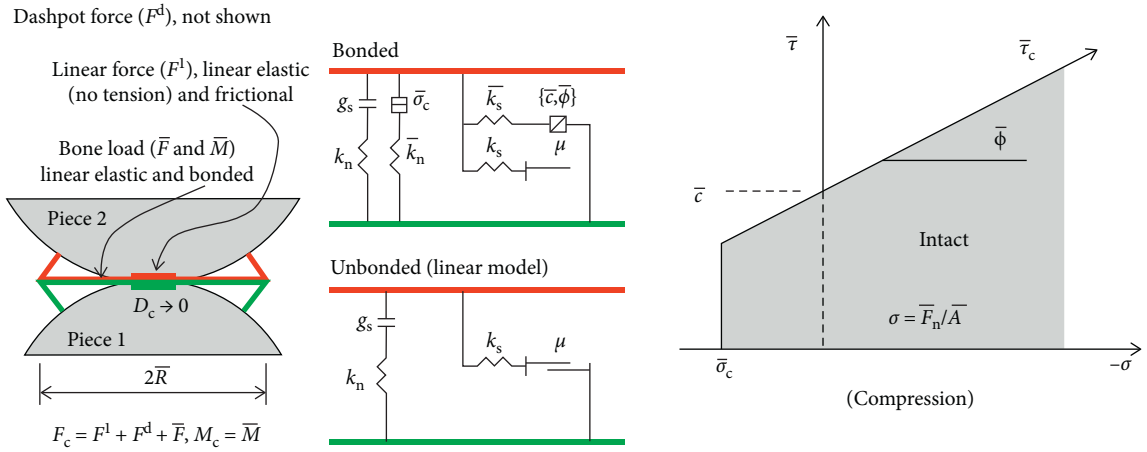

Figure 5: Mesoscopic contact model and failure criterion of the PBM.

radius of 1.2 mm. The particle diameter ratio is 1.66 [25]. The eight numerical models established by particle discrete element method are shown in Figure 6, in which the rubber mass fraction is 0, 5%, 10%, 15%, 20%, 25%, 30%, and 40%, respectively.

In order to eliminate the "cyclo-hoop effect" at both ends of the sample, the friction coefficient between the loading plate and the specimen is set to 0 during the numerical experiment to keep consistent with the sample boundary conditions in laboratory tests. The compiled code using the FISH language was used to achieve the uniaxial compression numerical experiment of the samples. The microdistribution of the particles and bond morphology in CRC materials are shown in Figure 7, in which the black parts represent the rubber particles, the yellow parts represent the sand particles and the white parts represent the bond formed by cement and coagulant.

3.3. Reverse Analysis and Determination of Mesoparameters. Based on the results of a large number of numerical experiments, combined with conclusions of other scholars' papers and monography [26–28], the mechanical mechanism of PBM and calibration basis of mesoscopic parameters can be summarized as follows: the macroelastic modulus is mainly related to the contact stiffness k_n of particle surfaces and the stiffness $\overline{k}_n$ of parallel bond, and the Poisson ratio is related to the normal/tangent stiffness ratio k_n/k_s of adjacent particles and the normal/tangent stiffness ratio $\overline{k}_n/\overline{k}_s$ of bond. And the peak strength is related to the shearing strength $\overline{c}$, $\overline{\Phi}$ of bond, and the friction coefficient μ between adjacent particles.

The inversion calibration of the CRC mesoparameters was conducted based on the results of laboratory experiments. The materials and processing technologies used in the preparation process of laboratory specimen are the same, and the only difference among them lies in the content of rubber particles; thus, the mesoparameters of particles and bonds in materials are the same in each sample. Firstly, the mesoparameters inversion calibration of sand particles based on the failure pattern and mechanical behavior of the NC was implemented, and then based on the established mesoparameters of the sand particles as well as the failure morphology and mechanical behavior of the sample with 40% rubber contents, the mesoparameters of rubber particles are established. The calibration curve of constitutive relation of materials is shown in Figure 8.

By combining the results of numerical tests and indoor tests and comparing the macromechanical parameters (Table 2) and failure modes (Figure 9) of the two materials, it can be concluded that the numerical model and experiment can ideally simulate and reveal the mechanical properties of the NC or the CRC, the established mesoparameters can reflect the mesomechanics and interaction of the internal particles within the composite material, and the mesoscopic physical and mechanical parameters of materials are shown in Table 3.

In order to verify the rationality and validity of the determined mesomechanical parameters, numerical simulations were conducted on other CRC samples based on the determined mesomechanical parameters, and the constitutive curves of each group were obtained. The comparison of constitutive curves obtained by laboratory experiments and those obtained by numerical simulations is shown in Figure 10. It can be found from the comparative analysis of the curve in the figure that the constitutive curves obtained from numerical experimentation are basically consistent with the laboratory test results, and the characteristics are as follows: with the increase of the rubber particles content, the compressive strength of the material shows a decreasing trend, the results are basically the same as that from laboratory tests, and the peak strain increases accordingly. It can be seen from the constitutive curve that the peak area of the stress-strain curve is gradually broaden with the increase of rubber particle content and the curve descending rate after the peak gradually become gentle. Since spherical particles are used in numerical simulation and the accidental factors in laboratory experiments cannot be excluded, the established model and microscopic parameters are considered reasonable and can reflect the microscopic mechanical response process of CRC composite materials with different rubber particles content, although there are some minor

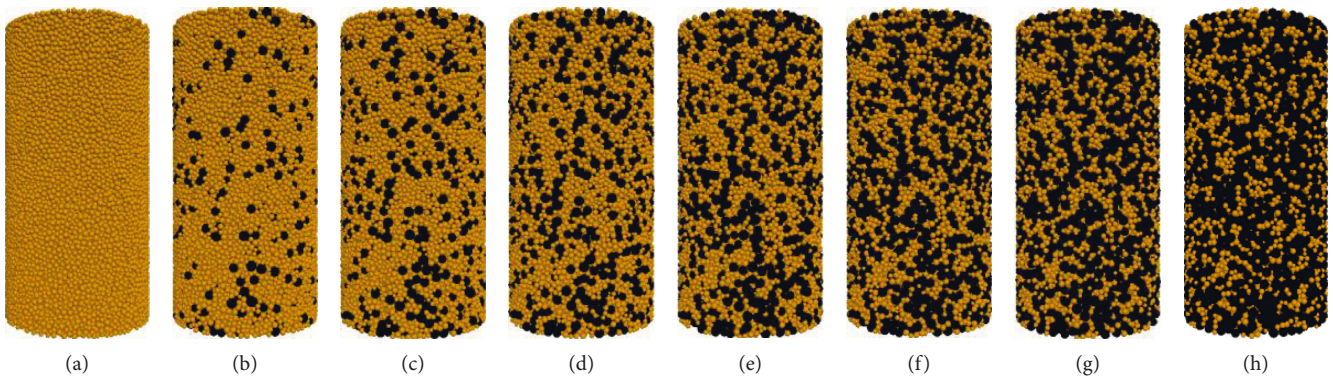

Figure 6: Numerical models of CRC with different rubber mass fraction. (a) 0% rubber. (b) 5% rubber. (c) 10% rubber. (d) 15% rubber. (e) 20% rubber. (f) 25% rubber. (g) 30% rubber. (h) 40% rubber.

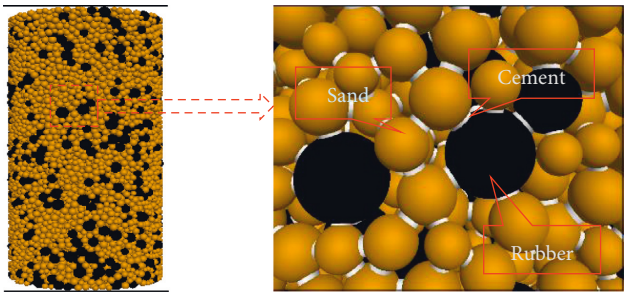

Figure 7: The numerical loading scheme and mesoscopic interface of samples.

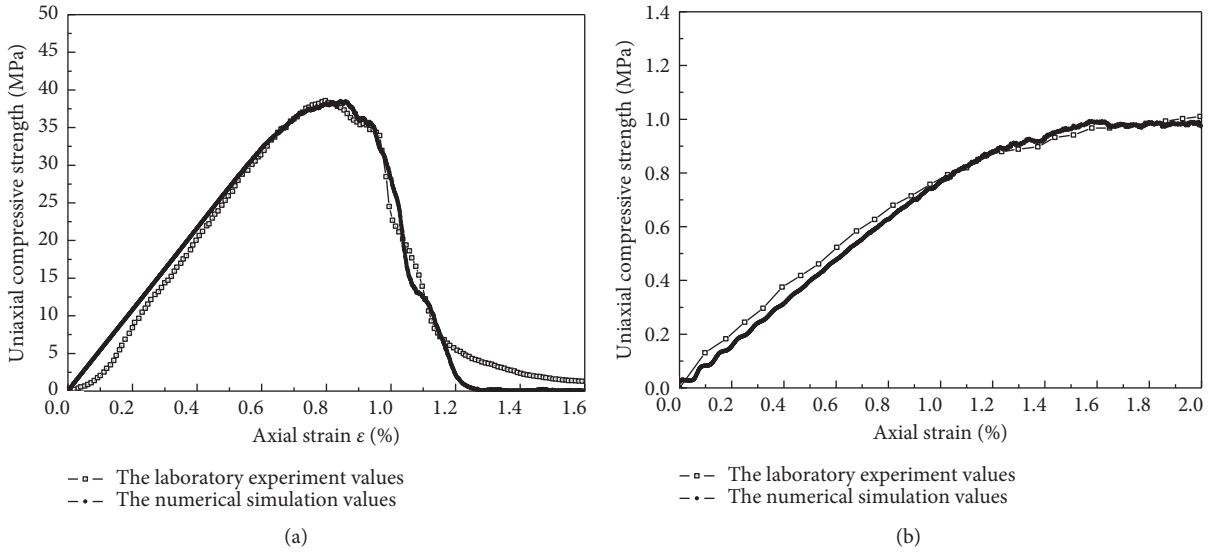

Figure 8: The calibration curve of constitutive relation of materials. (a) NC, 0% rubber. (b) CRC, 40% rubber.

Table 2: Mechanical parameters and PFC results.

Group	Compressive strength (MPa)	Peak strain (%)	Elasticity modulus (GPa)	Poisson ratio (l)
0%				
Laboratory	38.58	0.843	5.77	0.265
Simulation	38.9	0.915	5.72	0.261
40%				
Laboratory	1.15	1.63	0.065	0.386
Simulation	1.097	1.57	0.069	0.392

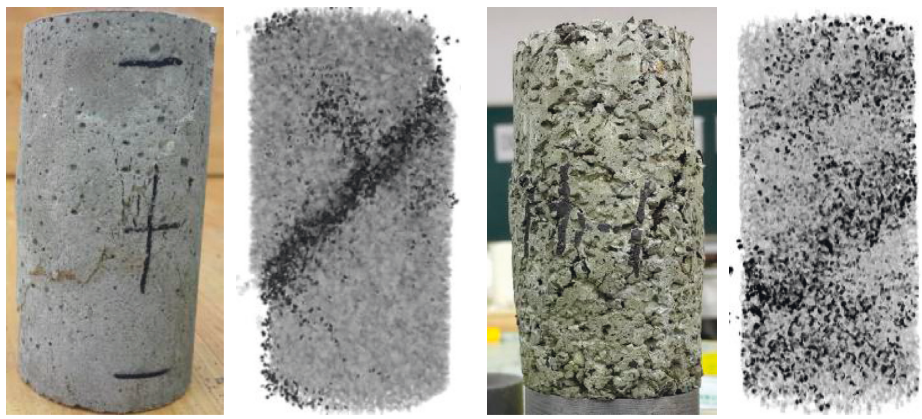

(a) (b)

Figure 9: The contrast figure of fracture morphology of laboratory (left) and simulation (right). (a) NC, 0% rubber. (b) CRC, 40% rubber.

Table 3: Mesomechanical parameters of the CRC.

Parameter	Sand	Rubber
The minimum size (mm)	0.8	1.2
The ratio of particle size (mm)	1.66	1.66
Density (kg/m^3)	2600	1200
The normal stiffness (N/m)	1.2e8	1.1e5
The stiffness ratio (l)	1.2	1.1
Friction coefficient (l)	0.42	0.98
Elastic modulus of bond (GPa)	1.72	0.102
Stiffness ratio of bond (l)	1.0	1.0
Tensile strength of bond (MPa)	65.1	6.52
Cohesive force of bond (MPa)	34.0	1.35
Friction angle of bond (°)	9	0

differences between the numerical simulation and the laboratory test in the peak phase and after peak phase of some materials.

4. Energy Evolution Rules and Microscopic Damage Mechanism

The failure process of materials is essentially the process of energy input, transformation, and dissipation. The failure process of CRC in uniaxial compression test is also an evolution process driven by energy as described below. Firstly, the loading plates of the testing machine input boundary energy to the concrete. As the loading progresses, the input energy can be gradually transformed into the releasable elastic strain energy, the sliding friction energy needed for the microcrack propagation and the fracture surface formation, and other dissipative energy such as particle kinetic energy and damping dissipation energy during the loading of samples.

4.1. The Microcracks Propagation in Damage Process of CRC. In the numerical model, the spherical particles are used to simulate aggregates in the CRC and the parallel bonds are used to simulate the cement and agglomerant between particles. When the shear stress between the particles is higher than its bond strength, the bond breaks and the particles slide, which can be considered as one microcrack generating inside the concrete. The process and rules of microcracks propagation of the CRC are simulated and analyzed by tracing the formation and number of broken bonds between particles.

Figure 11 shows the curve of the initiation and evolution of microcracks in CRC with different rubbers content. It can be seen from the figure that the microcrack number grows as "S" shape with the increase of strain during the loading process. The generating rate of cracks is relatively smooth in the beginning, then increases rapidly, and gradually becomes slow and stable after reaching the peak intensity. The time of cracks generation gradually lags behind with the increase of rubber contents, and the speed of cracks generation gradually decreases, resulting in a corresponding reduction in the total number of generated microcracks.

It can be seen from Figure 12 that the axial deformation at the initial microcrack formation of different CRC samples presents a "concave-upward" relationship with the of rubber content. The strain when the initial crack generation in the NC sample (without rubber) is 0.424%, and the corresponding strains of five groups of samples with 5%, 10%, 15%, 20%, and 25% rubber content are basically stable at about 0.2%, while the corresponding strains of the two groups of samples with 30% and 40% rubber content are 0.28% and 0.48%, respectively, showing an upward trend. The reasons for that are as follows: Since the higher cohesive force among sand particles in NC, the first microcrack generates when the stress between particles exceeds the ultimate strength of bond, resulting in the relatively large deformation of the NC. The addition of rubber reduces the bonding strength of the particles between sands and rubbers, which leads to the microcrack occurs when the strain is relatively small (e.g., five groups of samples with 5%, 10%, 15%, 20% and 25% rubber content). With the increase of rubber content, the deformation of rubber particles begins to be the main factor of high strain of samples, and the initial crack occurs when the samples have a relatively large deformation (e.g., two groups of samples with 30%, 40% rubber content).

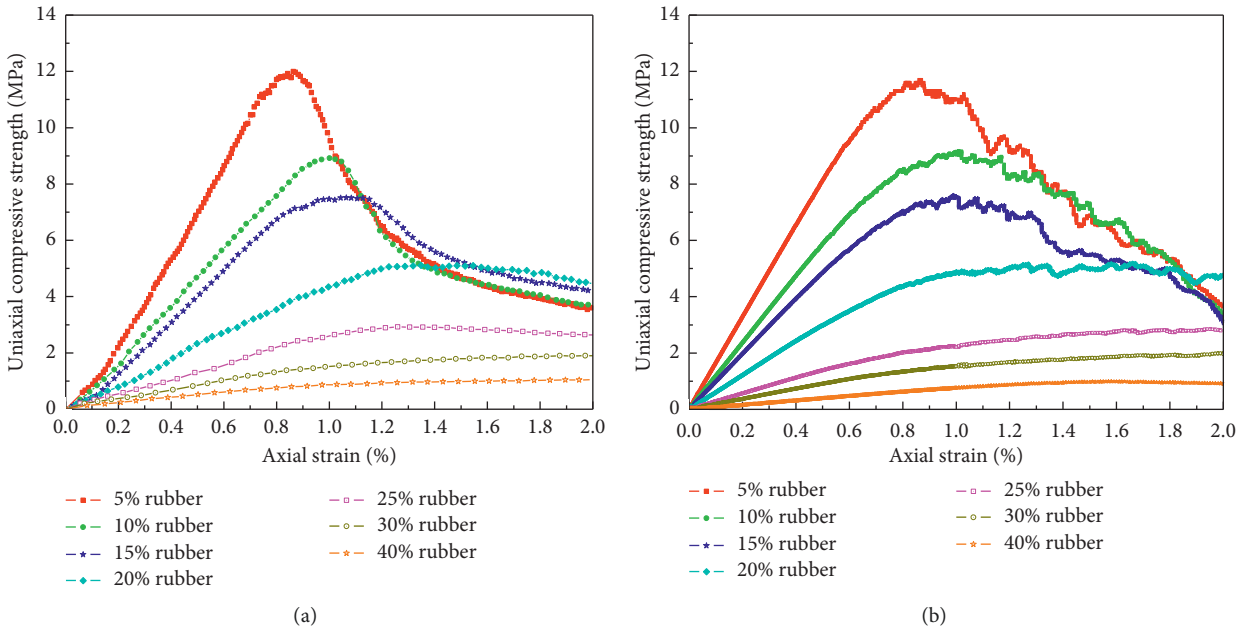

Figure 10: Comparison of constitutive curves obtained by laboratory experiments (a) and those obtained by numerical simulations (b).

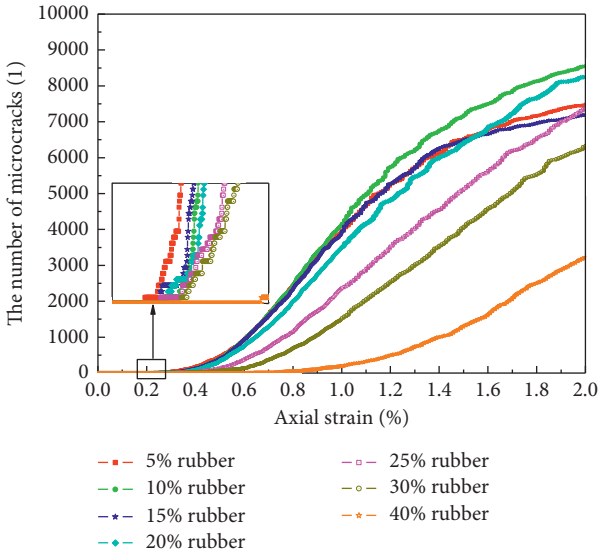

Figure 11: The initiation and evolution of microcracks.

The overall relationship between the number of microcracks generated and the content of rubber particles presents the "concave-downward" shape when the axial strain of samples is 2%. Accordingly, when the strain of materials is the same 2%, the number of cracks in the concrete without rubber is 7250, and the number of cracks in samples with 10% rubber and 20% rubber are, respectively, 8550 and 8250. Then the amount of cracks of CRC begins decrease with the increase of rubber contents, and the group with the largest rubber content has the least cracks which are 3230. The results show that the deformation and flexibility of rubber particles can effectively reduce the cracking of normal concrete and improve the overall stability of the material.

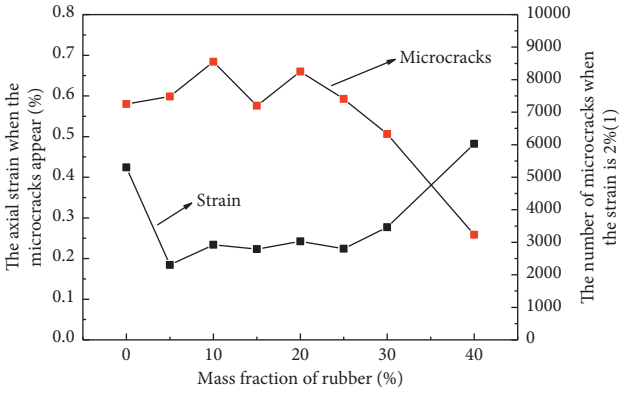

Figure 12: Relationship between microcracks, strain, and rubber content.

4.2. Rules of Energy Dissipation and Damage Mechanism. By using particle discrete element method to track and record the mechanical body energies, mechanical contact energies, and the formation of microcracks in the process of material destruction, the correlation between the energy dissipation and the damage mechanism of materials is analyzed. In the particle discrete element theory, the input energy U can be expressed as

$$U = U_{\text{pre}} + \left(F_1 \Delta U_1 + F_2 \Delta U_2\right), \tag{2}$$

where U_{pre} is the total input energy at the end of the last time step, and F_1, F_2 are the load of the up and down loading plates of the time step, respectively, and ΔU_1, ΔU_2 are the displacements of the loading plates, respectively, corresponding to the load at the time step. As for the PBM, the elastic strain energy U_e stored in the particle aggregate consists of strain energy E_k of contacting particles and the

strain energy $\overline{E}_k$ of parallel bond, and their formulas are as follows respectively:

$$E_k = \frac{1}{2}\left(\frac{\left(F_n^l\right)^2}{k_n} + \frac{\left\|F_s^l\right\|^2}{k_s}\right),$$
$$\overline{E}_k = \frac{1}{2}\left(\frac{\overline{F}_n^2}{\overline{k}_n\overline{A}} + \frac{\left\|\overline{F}_s\right\|^2}{\overline{k}_s\overline{A}} + \frac{\overline{M}_t^2}{\overline{k}_s\overline{J}} + \frac{\left\|\overline{M}_b\right\|^2}{\overline{k}_n\overline{I}}\right), \tag{3}$$

where F_n^l is the normal force of contacting particles, F_s^l is the tangential force of contacting particles, k_n is the normal stiffness of contacting particles, k_s is the shear stiffness of contacting particles, $\overline{F}_n$ is the normal force of bond, $\overline{F}_s$ is the tangential force of bond, $\overline{M}_t$ is the torsional moment, $\overline{M}_b$ is the bending moment, $\overline{A}$ is the cross-sectional area of bond, $\overline{I}$ is the moment of inertia of cross section of bond, and $\overline{J}$ is the polar moment of inertia of cross section of bond.

According to the second law of thermodynamics, the testing system is assumed to be a closed system without any heat exchange, the total input energy U consists of the elastic strain energy U_e stored in the system and the dissipated energy U_d which is necessary for the sample's internal damage and plastic deformation, and the formula is as follows:

$$U = U_e + U_d. \tag{4}$$

There are many forms to describe the macroscopic damage variable of rock and soil, and usually, it can be described as crack density, energy accumulation, fatigue life, mechanical parameter, and so on, and the method of degradation of dynamic elastic modulus [29] based on the effective stress and the strain equivalence principle is widely used, and the formula of the damage variable D_0 is

$$D_0 = 1 - \frac{\overline{E}}{E_0}, \tag{5}$$

where E_0 is the elastic modulus of materials at undamaged state, and $\overline{E}$ is the elastic modulus at the damage state. It can be seen from the expression that when $\overline{E}$ changes to E_0, D_0 is 0, and it is the original and undamaged state. Thus, the lager D_0 is, the more severe the damage of material is.

In the analysis of the particle discrete element model, based on the microstructure and the fracture mechanism of bond, the ratio of the number of fractured bonds N to the total number of bonds between particles N_0 is regarded as the mesoscopic damage variable D_m [30], and the expression is

$$D_m = \frac{N}{N_0}. \tag{6}$$

The damage variables and dissipation energy of eight groups of samples at different stages of the loading process are recorded and analyzed, as shown in Table 4, from which the relationship between them can be obtained as follows: When the CRC samples reach the peak strength, the variation trend of dissipation energy ratio is basically consistent with that of damage variable with the increase of rubber particles content, showing a trend of increase first and then decrease. The ratio of dissipation energy to total energy in the CRC group with 25% rubber content reaches the maximum of 41.4% and the corresponding damage variable is also the largest at 0.3, indicating that the overall structural stability of the sample is relatively the best and it needs to dissipate enough energy to reach its damage threshold. And other samples with a rubber content of 0%, 5%, or 10% have the relatively high integral strength and low resist deformation ability due to the less rubber content, and the brittle failure occurs when the damage variable is low. Similarly, samples with a rubber content of 30% and 40% also suffer destruction when the damage variable is relatively small due to the low bonding strength between the particles caused by the incorporation of more rubber particles, and the corresponding dissipation energy ratio is also relatively low.

The statistical analysis of damage variables and dissipation energy is carried out in the postpeak stage of material destruction, which shows that the damage variable and the dissipative energy ratio after the destruction of materials increase with the increase of rubber content. The proportion of the dissipated energy increases from 81.7% to 98.4% as the rubber content increases, showing that most of the total input energy of CRC is dissipated after the material reaches destructive stability and the rest energy is stored in the retained samples in the form of elastic strain energy among particles.

The microdamage variable at the peak strength is used as the material's damage threshold D_{cri}, which can be seen at formula (7), and it is defined as the ratio between the number of broken bonds N_{cri} at the peak strength and the total number of bonds N_0. The damage threshold represents the circumstance of internal damage when the material reaches the ultimate strength, that is, the critical value of structural damage in the material under external load. And when the damage degree of material exceeds the value, the structure is completely destroyed and loses its bearing capacity.

$$D_{cri} = \frac{N_{cri}}{N_0}. \tag{7}$$

Figure 13 shows the relationship between the damage threshold and the number of microcracks at the peak strength of CRC samples with different rubber contents. It can be seen from the figure that with the increase of rubber content, the total number of bonds in samples shows a decreasing trend with the numbers being 51510, 39896, 38364, 37480, 35034, 31712, 29564, and 22847, respectively, and the corresponding number of microcracks at the peak presents a "increase first and then decrease" trend with the numbers being 1510, 2950, 4215, 4420, 6310, 9610, 7490, and 1520, respectively. The damage threshold also presents the "increase first and then decrease" trend with the addition of the rubber contents, and the damage thresholds are 0.029, 0.074, 0.11, 0.118, 0.18, 0.3, 0.253, and 0.067, respectively. Wherein the group with rubber content of 25% has the largest damage threshold which is 0.3, showing that this sample reaches its ultimate strength when the number of cracks accounts for 30% of the number of total bonds and has the maximum overall utilization; that is, only when the overall damage degree of this sample reaches 30%, can it lose the bearing capacity.

Table 4: Statistics for the damage variable and dissipation energy.

Groups/mass fraction of rubber (%)	In the peak stage of the materials				In the stable stage of materials destruction			
	Input energy (J)	Dissipation energy (J)	Damage variable	Dissipative energy ratio (%)	Input energy (J)	Dissipation energy (J)	Damage variable	Dissipative energy ratio (%)
0	36.5	9	0.029	24.7	53	43.3	0.14	81.7
5	11.6	2.81	0.074	24.2	30.4	26.36	0.196	86.7
10	11	2.96	0.11	26.9	25.7	22.31	0.231	86.8
15	9.98	3.02	0.118	30.3	20.6	18.41	0.194	89.4
20	10.4	3.97	0.18	38.2	22.3	20.25	0.285	90.8
25	11.6	4.8	0.3	41.4	15.3	14.28	0.372	93.3
30	6.31	2.3	0.253	36.5	11.0	10.38	0.386	94.4
40	1.8	0.36	0.067	20	3.63	3.57	0.211	98.4

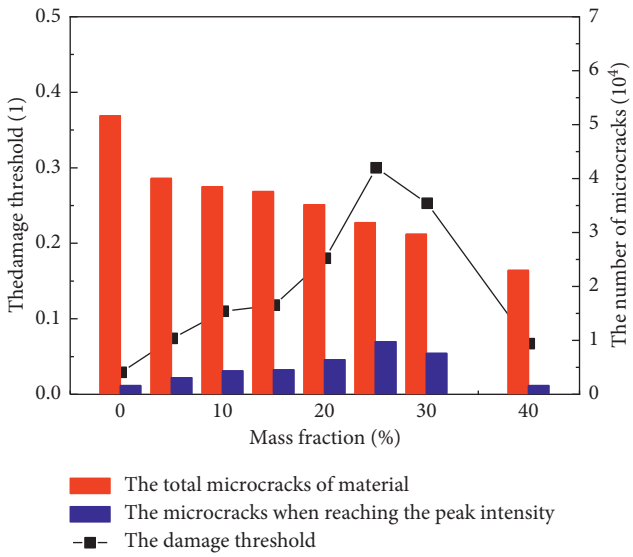

Figure 13: Relationship between damage threshold, number of microcracks, and content of rubber particles.

As for the group without rubber contents, it reaches the ultimate strength when the damage thresholds value is 0.029, showing that the material in this group has reached the ultimate bearing capacity when the overall damage degree comes to 2.9%. Similarly, the two groups with rubber content of 5% and 40% have been completely destroyed when their overall damage degrees are less than 10%.

The elastic strain energy release ratio E_{rt} is defined from the perspective of energy to describe the energy release state of the material after the peak. E_{rt} is defined as the ratio that the absolute value of difference value between the maximum elastic strain energy stored in the materials E_p and the elastic strain energy E_s at the time of the stability of destroy compared with the absolute value of the corresponding strain difference value, which represents the release value of the elastic strain energy in the unit strain after the sample reaches the peak strength. The bigger the E_{rt} is, the bigger the energy release value in the unit strain is after material the reaches the ultimate bearing capacity, and the more brittle the material is, the more severe the degree of damage is. Oppositely, the smaller the value of E_{rt} is, the more pliable and tough the material is and the more smooth and steady the degree of damage is after the material reaches the peak strength.

$$E_{rt} = \left|\frac{\Delta E}{\Delta \varepsilon}\right| = \left|\frac{E_p - E_s}{\varepsilon_p - \varepsilon_s}\right|. \quad (8)$$

Figure 14 shows the relationship between the different rubber contents in CRC and the corresponding elastic strain energy release ratio. It can be seen that the elastic strain energy release ratio comes to 48.8 J/% after the concrete reaches the peak strength without adding rubbers. When rubber particles are added to the concrete, the energy release ratio decreases sharply, and presents negative exponential function type with the downtrend of first sharp and then slow, and other groups' energy release ratios are 8.83 J/%, 7.54 J/%, 7.36 J/%, 6.17 J/%, 5.47 J/%, 3.29 J/%, and 1.15 J/%, respectively, which can quantitatively describe the relation between the energy release rate and the rubber particle contents by using the fitting function $y = 37.53\exp(-5.622x) + 11.27\exp(-0.036x)$ in the figure. And the fitting effect is good with the fitting variance value of 0.9971. The analysis of the fitting curve shows that the presence or absence of the rubber particles has more sensitive effect to the energy release ratio than the content of the rubber particles, indicating that rubber materials can significantly reduce the brittleness of concrete and improve the overall flexibility and ductility of materials.

4.3. The Correlation of Material Damage and Energy Evolution. Figure 15 shows the correlation rule between damage process and energy evolution in the group without rubber contents (0% of the rubber particle contents, (a)) and the group with maximum damage threshold (25% of the rubber particle contents, (b)). The damage mechanism and the energy evolution rule of the CRC composite materials and normal concrete materials are analyzed by taking the group with maximum damage threshold and the group without rubber contents as representatives.

The analysis of Figure 15 can be obtained:

In the initial loading phase (OA), the boundary input energy of the two materials both shows a slowly increasing trend, and basically coincide with the elastic strain energy. The sliding friction energy, kinetic energy, and other dissipated energy are basically zero and can be neglected. The boundary input energy of materials is completely transformed into the elastic strain energy stored in the materials, and no microcracks are generated in this phase.

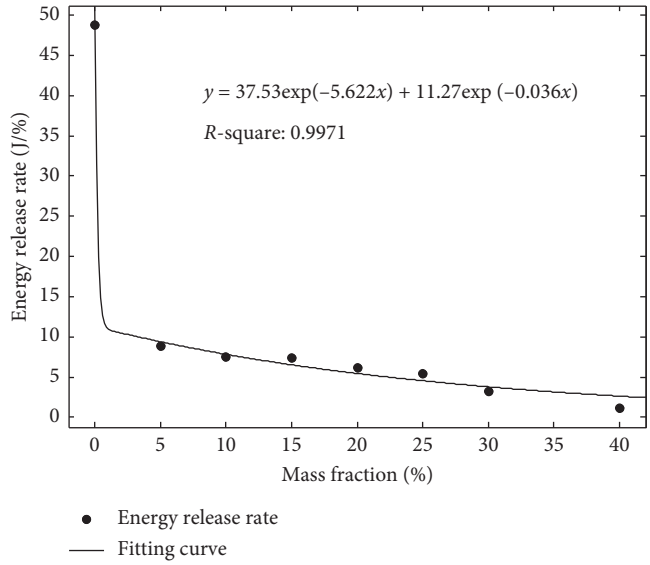

Figure 14: The relationship between energy release ratio of CRC and rubber content.

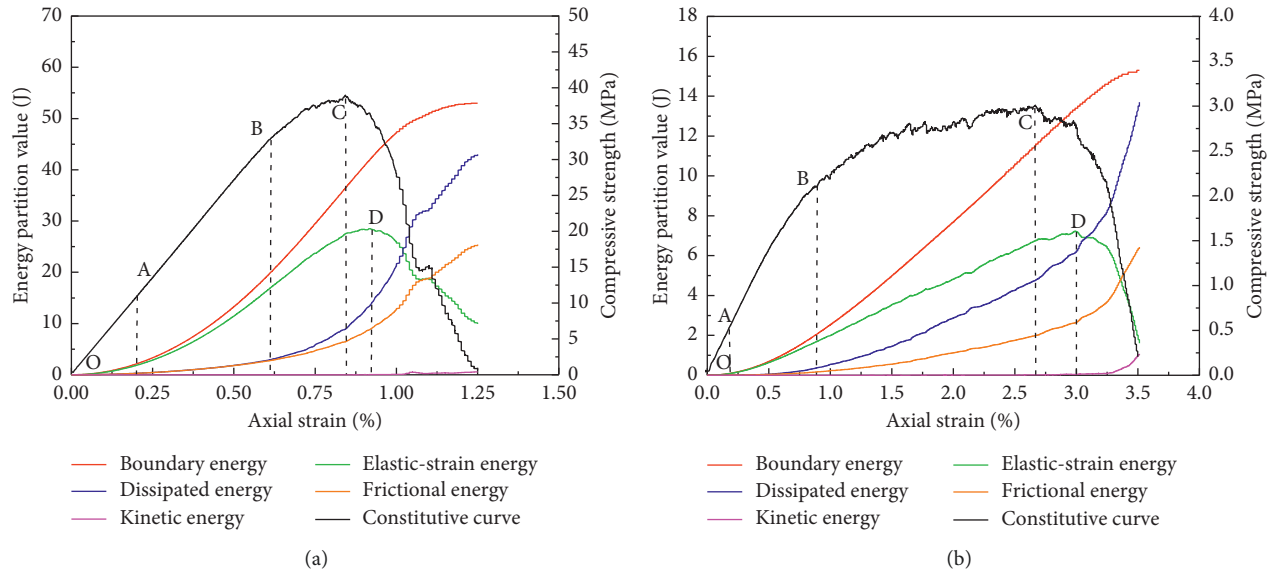

Figure 15: The relationship between the mesoscopic energy evolution law of CRC and their constitutive curves. (a) The rubber mass fraction is 0. (b) The rubber mass fraction is 25%.

In the linear elastic phase (AB), the input energy and elastic strain energy begin to separate, and both of them show a slow development trend in the shape of "upward concave." The elastic strain energy accumulates and stores gradually, the microcracks in the materials begin to occur, and the sliding friction energy and other dissipated energy begin to increase slowly. The dissipation energy curve basically coincides with the frictional energy curve, showing the dissipated energy is mainly used for sliding friction consumption of materials at this phase. Macroscopically, the stress-strain curve shows the linear elasticity, which is the stable development stage of the materials.

In the yield phase (BC) of materials, the curves of the input energy and the elastic strain energy are completely separated; both of them show a rapid linear growth in general, and the growth rate of input energy is larger than that of the elastic strain energy. The curves of sliding friction energy and dissipated energy begin to separate and grow rapidly in a shape of "upward concave," and a large number of microcracks are rapidly generated inside the material. It indicates that a large amount of damage occurs in the microstructure of the material at this phase, and the particles are mutually slipping and moving, and the dissipated energy represented by the sliding friction energy between particles increases significantly, which shows the materials reach the ultimate bearing capacity at the point C.

In the postpeak phase (after the point C), the curve of material constitutive relation lags behind that of energy

evolution as energy is the driving factor for damage and fracture of materials. The boundary input energy continues to increase in a linear trend and tends to be gentle in the later phase, while the elastic strain energy continues to grow in a shape of "upward convex," and begins to decline after reaching the peak at the point D. The sliding friction energy, kinetic energy, and other dissipated energy increase rapidly and gradually tend to be stable in the later phase, and the generation rate of microcracks gradually reduces to zero.

5. Discussion

The stress-strain relationship of CRC materials is basically consistent with the development trend of their elastic strain energy, but the stress-strain curve lags behind the development of elastic strain energy, which indicates that energy is an important driving factor for the damage and fracture of materials. The CRC with 25% of the rubber mass has a larger yield phase and smaller elastic strain energy release ratio than the NC, which can be explained as the addition of rubber particles makes more external input energy to be converted into dissipative energy required for microcracks propagation and sliding friction between particles and released step by step.

The purpose of CRC materials research is to improve the deformation capacity and toughness as far as possible on the basis of maintaining a certain compressive strength to prevent sudden failure of the project. The size of rubber particles used in this study is 3–5 mm, and when the rubber mass fraction is 25%, the coordination between the strength and deformation of the material was the best. In the later research, experiments can be carried out on different CRC rubber particle sizes and different rubber treatment methods to obtain a more ideal CRC ratio scheme with better mechanical and deformation capacity.

The acoustic emission experiment can be used to study the micromechanical failure mechanism of CRC materials to verify the effectiveness and accuracy of conclusions obtained by this method.

Different pretreatment methods of rubber particles before CRC production may affect the overall compatibility, strength, and other properties of the material. We will try a variety of different treatment methods of rubber particles in the later research, including untreated rubber particles, acid treatment, and mixed treatment, etc., to study the effect of functionalization of rubber particle surface on the compatibility of CRC material components. Thus, a better treatment method of rubber particles may be obtained to improve the overall strength and deformation performance of CRC.

6. Conclusions

In this paper, the energy evolution law and mesodamage mechanism of CRC (crumb rubber concrete) are investigated both by laboratory experiments and the particle discrete element method, and the energy evolution behavior and damage characteristics of NC (normal concrete) are compared and analyzed.

The results of this investigation are summarized as follows:

(1) With the increase of rubber particles content, the axial deformation of CRC gradually increases, the integrity of the samples is better after reaching its ultimate bearing capacity, and the failure form is gradually changed from a form of single sloping and complete plane to a form of short and dispersed cracks. The proposed fitting functions can well fit the relationship among the compressive strength, elastic modulus, and the rubber particles content, respectively.

(2) The mesoscopic physical and mechanical parameters of the CRC with rubber particles and sand particles as the main aggregate are analyzed and determined, which can better simulate the macroscopic mechanics and deformation characteristics of CRC materials.

(3) It is considered that the mesoscopic damage threshold of CRC materials with different rubber contents has a strong correlation with the proportion of dissipated energy at the peak strength, and both of them show the tendency of increasing first then decreasing with the increase of rubber mass.

(4) The damage threshold of the group with 25% of the rubber mass is the largest, and it is 30%, and the corresponding dissipated energy ratio at the peak strength is 41.4%, which indicates that the composite materials need to dissipate 41.4% of the input energy, and when its damage state reaches 30% of the overall integrity, it will reach the ultimate bearing capacity.

(5) The elastic strain energy release ratio is proposed to describe the elastic strain energy released by the unit strain after the material reaches the ultimate bearing capacity. The relationship between elastic strain energy release ratio of CRC and rubber particle contents is obtained and fitted by the negative exponential function $y = 37.53\exp(-5.622x) + 11.27\exp(-0.036x)$. It is considered that the rubber composition can significantly reduce the energy release ratio and obviously improve the flexibility and ductility of the composite concrete materials.

Data Availability

The data used to support the findings of this study are available from the corresponding author upon request.

Conflicts of Interest

The authors declare that there are no conflicts of interest regarding the publication of this paper.

Acknowledgments

The authors would like to acknowledge the support of the National Natural Science Foundation of China (nos. 51474135 and 41272325). We are also grateful to the graduate student Jun Zhu for participating in the experimental work.

References

[1] N. N. Eldin and A. B. Senouci, "Rubber-tire particles as concrete aggregate," *Journal of Materials in Civil Engineering*, vol. 5, no. 4, pp. 478–496, 1993.

[2] Z. K. Khatib and F. M. Bayomy, "Rubberized portland cement concrete," *Journal of Materials in Civil Engineering*, vol. 11, no. 3, pp. 206–213, 1999.

[3] Y. Yu and H. Zhu, "Influence of rubber size on properties of crumb rubber mortars," *Materials*, vol. 9, no. 7, p. 527, 2016.

[4] N. Segre and I. Joekes, "Use of tire rubber particles as addition to cement paste," *Cement and Concrete Research*, vol. 30, no. 9, pp. 1421–1425, 2000.

[5] R. Wang, P.-M. Wang, and X.-G. Li, "Physical and mechanical properties of styrene-butadiene rubber emulsion modified cement mortars," *Cement and Concrete Research*, vol. 35, no. 5, pp. 900–906, 2005.

[6] I. B. Topçu and N. Avcular, "Analysis of rubberized concrete as a composite material," *Cement and Concrete Research*, vol. 27, no. 8, pp. 1135–1139, 1997.

[7] İ. B. Topçu, "Assessment of the brittleness index of rubberized concretes," *Cement and Concrete Research*, vol. 27, no. 2, pp. 177–183, 1997.

[8] I. B. Topçu, "The properties of rubberized concretes," *Cement and Concrete Research*, vol. 25, no. 2, pp. 304–310, 1995.

[9] F. Hernández-Olivares, G. Barluenga, M. Bollati, and B. Witoszek, "Static and dynamic behaviour of recycled tyre rubber-filled concrete," *Cement and Concrete Research*, vol. 32, no. 10, pp. 1587–1596, 2002.

[10] O. Youssf, J. E. Mills, and R. Hassanli, "Assessment of the mechanical performance of crumb rubber concrete," *Construction and Building Materials*, vol. 125, pp. 175–183, 2016.

[11] H. Zhu, C. Liu, Y. Zhang, and Z. Li, "Effect of crumb rubber proportion on compressive and flexural behavior of concrete," *Journal of Tianjin University*, vol. 40, no. 7, pp. 761–765, 2007, in Chinese.

[12] M. Zhou, H. Zhu, and Z. Xue, "Experimental on compressive strength of rubber aggregate plastic concrete," *Journal of Civil, Architectural and Environmental Engineering*, vol. 33, no. S1, pp. 74–78, 2011, in Chinese.

[13] M. Zhou, H. Zhu, L. Ai, Z. Xue, and Y. Wu, "Effect of volumetric percentage of rubber-particles on properties of plastic concrete," *Journal of Building Materials*, vol. 12, no. 5, pp. 563–567, 2009, in Chinese.

[14] L. Yang, *Exploration on Microstructure and Structural Theory of Crumb Rubber Concrete*, Tianjin University, Tianjin, China, 2010, in Chinese.

[15] F. Liu, D. Pan, L. Li, and Y. Chen, "Numerical simulation on micro-level of stress and strength in crumb rubber concrete," *Journal of Building Materials*, vol. 11, no. 2, pp. 144–151, 2008, in Chinese.

[16] F. Liu, G. Zhong, X. Xia, and L. Li, "Mechanical analysis of rubberized concrete subjected to uniaxial compression on meso-level," *Journal of Building Materials*, vol. 13, no. 6, pp. 733–738, 2010, in Chinese.

[17] F. Liu, H. Huang, X. Xia et al., "Mechanical test on modified concrete with recycled plastic particles and its numerical simulation," *Journal of Building Materials*, vol. 14, no. 2, pp. 173–179, 2011, in Chinese.

[18] W. Liu, *Frost Resistance Research of Concrete Containing Scrap Rubber Powder*, Dalian University of Technology, Dalian, China, 2011, in Chinese.

[19] Y. Yuan and L. Zheng, "Experimental study on dynamic properties of rubberized concrete," *Journal of Tongji University (Natural Science)*, vol. 36, no. 9, pp. 1186–1190, 2008.

[20] J. Xu, Z. Li, X. Luo, B. Leng, and Z. Liu, "A comparative study of the static and dynamic compression strength of rubber powder concrete," *Journal of Building Materials*, vol. 17, no. 6, pp. 1015–1019, 2014, in Chinese.

[21] Y. Guo, F. Liu, G. Chen, G. Zeng, and F. Liu, "Experimental investigation on impact resistance of rubberized concrete," *Journal of Building Materials*, vol. 15, no. 1, pp. 139–144, 2012, in Chinese.

[22] P. A. Cundall and O. D. L. Strack, "A discrete numerical model for granular assemblies," *Géotechnique*, vol. 29, no. 1, pp. 47–65, 1979.

[23] W. Qiao, L. Wang, D. Lin et al., "Research on optimum of mix proportion of rubber concrete with orthogonal experimental design method," *Concrete*, no. 10, pp. 89–92, 2014, in Chinese.

[24] Itasca Consulting Group Inc., *Manual of Particle Flow Code in 3-Dimension (Version 5.0)*, Itasca Consulting Group Inc., Minneapolis, MN, USA, 2016.

[25] E. Z. Lajtai, E. J. S. Duncan, and B. J. Carter, "The effect of strain rate on rock strength," *Rock Mechanics and Rock Engineering*, vol. 24, no. 2, pp. 99–109, 1991.

[26] J. Xu, Z. Xie, and H. Jia, "Simulation of mesomechanical properties of limestone using particle flow code," *Rock and Soil Mechanics*, vol. 31, no. S2, pp. 390–395, 2010, in Chinese.

[27] G. Zhang, H. Li, X. Xia et al., "Effects of microstructure and micro parameters on macro mechanical," *Chinese Journal of Rock Mechanics and Engineering*, vol. 35, no. 7, pp. 1341–1352, 2016, in Chinese.

[28] X. Xu, D. Ling, Y. Chen, and B. Huang, "Correlation of microscopic and macroscopic elastic constants of granular materials based on linear contact model," *Chinese Journal of Geotechnical Engineering*, vol. 32, no. 7, pp. 991–998, 2010, in Chinese.

[29] J. Lemaitre, "Evolution of dissipation and damage in metals submitted to dynamic loading," in *Proceedings of the ICMI*, pp. 151–157, Kyoto, Japan, 1968.

[30] D. Cen and D. Huang, "Mechanical responses and energy dissipation mechanism of rock specimen with a single fissure under static and dynamic uniaxial compression using particle flow code simulations," *Chinese Journal of Rock Mechanics and Engineering*, vol. 32, no. 9, pp. 1926–1936, 2013, in Chinese.